Aerosol Route to TiO 2 –SiO 2 Catalysts with Tailored Pore Architecture and High Epoxidation Activity

Valentin Smeets, Cédric Boissière, Clément Sanchez, Eric M. Gaigneaux, Elise Peeters, Bert Sels, Michiel Dusselier, Damien P. Debecker

Aerosol Route to TiO2–SiO2 Catalysts with Tailored Pore Architecture and High Epoxidation Activity

Valentin Smeets,[†] Cédric Boissière,[‡] Clément Sanchez,[‡] Eric M. Gaigneaux,[†] Elise Peeters,[§] Bert F. Sels,[§] Michiel Dusselier,[§] and Damien P. Debecker*[,†]

[†]Institute of Condensed Matter and Nanosciences (IMCN), UCLouvain, Place Louis Pasteur, 1, Box L4.01.09, 1348 Louvain-la-Neuve, Belgium

[‡]Sorbonne Université, CNRS, Collège de France, PSL Research University, Laboratoire Chimie de la Matière Condensée de Paris, LCMCP, 4 Place Jussieu, F-75005 Paris, France

[§]Centre for Surface Chemistry and Catalysis, KU Leuven, Celestijnenlaan 200F, 3001 Leuven, Belgium

ABSTRACT: Herein, we present the aerosol-assisted sol − gel preparation of hierarchically porous TiO 2 − SiO 2 catalysts having a spherelike shell morphology and a high Ti dispersion. In order to control the porosity at the micro-, meso-, and macrolevels, we use the evaporation-induced self-assembly (EISA) of a surfactant, possibly combined with polymer beads as hard templates. These catalysts are tested for the epoxidation of cyclohexene with cumene hydroperoxide as the oxidant, and their performance is compared to the reference TS-1 zeolite. The high catalytic performance observed with the catalysts prepared by aerosol stems from their high speci fi c surface area, but also from the short di ff usion path length generated by the meso-/macropore architecture which provides entryways for bulky reactants and products. Besides, these materials can incorporate a higher Ti loading than TS-1 zeolite, while ensuring a good control over the Ti speciation. Thus, the unique features of the aerosol process which is also known to be scalable allow us to prepare catalytic materials with high epoxidation activity, also for bulky olefins.

1. INTRODUCTION

The simultaneous control over active site speciation and texture is a key to develop high-performance heterogeneous catalysts. These parameters indeed dictate the intrinsic activity of the catalyst and the efficiency of the mass transport within the solid, and it is challenging to optimize both aspects simultaneously.

A common illustration of this dilemma is the titanium-containing zeolite TS-1 which has been industrialized in the mid-eighties as a selective oxidation catalyst.[1] More particularly, the combination of TS-1 and hydrogen peroxide H_2O_2 has been mainly used in two industrial applications, namely, phenol hydroxylation and cyclohexanone ammoximation,[2] the latter being involved in the production of caprolactam, an important molecule used in the production of nylon 6.[3] TS-1 is also an efficient catalyst for the epoxidation of lower olefins with H_2O_2, even at low temperature and in the presence of water, thus bringing an environmentally friendly alternative to typical epoxidation processes (e.g., for propylene oxide production).[4] For these selective oxidation reactions, isolated Ti species in tetrahedral coordination are known to be the active sites.[4,5]

Despite these appealing characteristics, TS-1 suffers from two drawbacks: (i) Ti loading in the MFI crystal structure of TS-1 is commonly limited to a maximum of 2.5% (here and after the loading is expressed as mol Ti/(mol Ti + mol Si) × 100%)[6,7] and (ii) the intrinsic microporosity of the zeolite framework is not compatible with the size of bulkier olefins—such as cyclohexene, for example—oxidizing agents, and reaction products for which diffusion in and out the pores is strongly hampered.[2,8]

Extending the versatility of Ti-containing catalysts to a wider range of substrates and conditions is a challenge that can be tackled by two approaches.[9] On the one hand, if the microporosity is assumed to be inaccessible, it is possible to enhance the activity of TS-1 by decreasing the size of the zeolite crystals so as to increase the proportion of the external surface.[10] In such case, small TS-1 crystals can be advantageously dispersed at the surface of another porous solid support with the desired pore size and pore architecture.

For example, Liu et al.[11] proposed the in situ hydrothermal synthesis of a hierarchically porous TS-1/modified diatomite composite, exploited in the hydroxylation of toluene and phenol with H_2O_2. A similar idea is to prepare hierarchical materials based on the TS-1 structure supplemented with larger pores[12] or to shape the zeolite in the form of TS-1 nanosheets[13] or pillared TS-1.[14] However, the conversion is still limited by the titanium loading and the microporosity of TS-1.

A second way out is to incorporate titanium atoms in silica-based materials with controlled texture, either by producing small nonporous particles (e.g., via flame spray pyrolysis[15−17]) or by designing materials with larger pores[18,19] (e.g., Ti−β zeolites,[20] Ti−MCM-41,[21] TiO_2−SiO_2 aerogels, Ti−SiO_2 macrocellular foams,[22] and[23,24] TiO_2−SiO_2 xerogels[25−28]). Sol−gel chemistry[29,30] represents an important toolbox for the bottom-up preparation of such mesoporous catalysts.[31,32] The most significant progress in this direction was obtained thanks to the development of templating strategies (e.g., evaporation-induced self-assembly, EISA[33,34]), or specific drying strategies.[35] However, in these cases, controlling the transition-metal dispersion remains a challenge owing to the different hydrolysis and condensation rates for Ti and Si precursors. This can be tackled with specific strategies, including the use of reactivity modifiers,[36,37] or nonhydrolytic routes,[38] for instance. Nevertheless, the fine tuning of the porosity at the micro-, meso-, and macrolevels is still often limited by the numerous and time-consuming steps required to generate, control, and preserve the pore architecture.

Currently, the aerosol-assisted sol−gel process is emerging as a versatile and highly potent method for the preparation of advanced nanomaterials,[39,40] in particular heterogeneous catalysts (Figure 1).[41] Such a bottom-up preparation route was shown particularly powerful to control simultaneously the texture, the composition, and the homogeneity of various types of mixed oxide catalysts,[42−47] including TiO_2−SiO_2 formulations.[12,48] On the basis of the fast drying of the aerosol precursor solution, the method exploits the quenching of the condensation kinetics, leading to highly homogeneous formulations. Besides, the porosity can be easily controlled by the incorporation of templating agents [e.g., chitin nanorods[48] or cetrimonium bromide (CTAB)/tetrapropylammonium hydroxide (TPAOH)[12]] in the precursor solution.

Here, we propose to leverage on this aerosol strategy to obtain, in one step and in a continuous fashion, spherelike particles of TiO_2−SiO_2 catalysts with both tunable hierarchical porous architecture and highly dispersed Ti species. To control the texture at different levels, we use the EISA of a surfactant (Figure 1a), possibly combined with hard templates, during the aerosol process. The advantageous properties of these materials are exploited in a model epoxidation reaction and compared to the reference TS-1.

2. EXPERIMENTAL SECTION

2.1. Preparation of the Materials. The catalysts were prepared with a 4% Ti loading starting from precursor solutions prepared as follows:

Aer_15: for 1 g of calcined material, 0.231 g of titanium butoxide (TiBuO, Fluka, 99%) was first added dropwise to 1.255 g of 40% (w/w) aqueous TPAOH (Merck) under stirring. After 10 min of mixing, 5.169 g of distilled H_2O was added, followed by 10 min stirring and the subsequent addition of 3.351 g of tetraethyl orthosilicate (TEOS, Sigma, 98%). The resulting solution was kept overnight under vigorous stirring to hydrolyze the precursors and further aged for 15 h at 70 °C in a closed vessel. Pluronic F127 (0.995 g, BASF) was then added and the solution was thoroughly mixed for at least 1 h. The composition of the resulting clear yellowish solution was 1 SiO_2/0.042 TiO_2/0.16 TPAOH/0.005 F127/17 H_2O/4 EtOH. For **Aer_15_2%**, the precursor solution was prepared by the same procedure using 0.116 g of TiBuO, 1.263 g of 40% aq TPAOH, 5.204 g of distilled H_2O, 3.445 g of TEOS, and 1.022 g F127. The final composition was 1 SiO_2/0.02 TiO_2/0.15 TPAOH/0.005 F127/16 H_2O/4 EtOH.

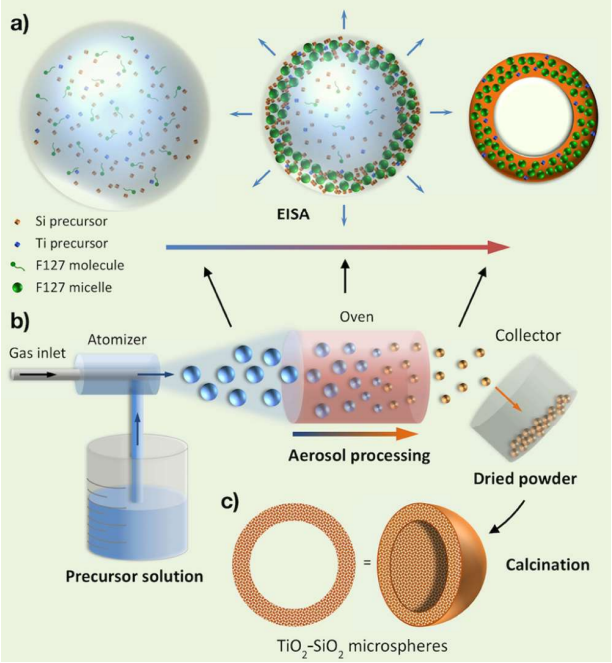

Figure 1. Preparation of mesostructured TiO_2−SiO_2 microspheres by the so-called Type IIIc aerosol technique.[41] (a) Illustration of the EISA mechanism (TPAOH has been omitted for clarity); (b) schematic representation of the aerosol setup; (c) illustration of the texture and morphology of the calcined material in the typical conditions used (see the Experimental Section for further details).

Aer_20: the precursor solution was prepared using 0.231 g of TiBuO, 1.673 g of 40% aq TPAOH, 4.919 g of distilled H_2O, 3.352 g of TEOS, and 0.995 g F127. The final composition was 1 SiO_2/0.042 TiO_2/0.21 TPAOH/0.005 F127/17 H_2O/4 EtOH.

Aer_25: the precursor solution was prepared using 0.231 g of TiBuO, 2.090 g of 40% aq. TPAOH, 4.665 g of distilled H_2O, 3.350 g of TEOS, and 0.994 g of F127. The final composition was 1 SiO_2/0.042 TiO_2/0.26 TPAOH/0.005 F127/17 H_2O/4 EtOH.

The precursor solutions were sprayed by Büchi Mini Spray Dryer B-290 with an air pressure of 4 bars. The aerosol was dried by passing through a glass reactor heated at 220 °C (**Aer_15**, **Aer_20**, and **Aer_25**) or 75 °C (**Aer_PS** and **Aer_PMMA**). The obtained powders were aged at 70 °C overnight and then calcined in air at 550 °C for 5 h (5 °C/min).

Monodisperse colloidal suspension of poly(methyl methacrylate) (PMMA) was prepared following a surfactant-free synthesis using ammonium peroxodisulfate as a thermal initiator according to the procedure of Goodwin et al.[49] The synthesis was carried out at 90 °C in a double envelop reactor thermostated with a waterbath circulation. After synthesis, the colloidal suspension was filtered through a filter paper in order to remove few particles aggregates produced onto the edge of the reactor. The obtained PMMA latex exhibits a mean particle size distribution centered at 278 nm [with full width at half-maximum (fwhm) of 63 nm].

Monodisperse polystyrene (PS) colloidal suspension was obtained following an emulsion polymerization route initiated by potassium

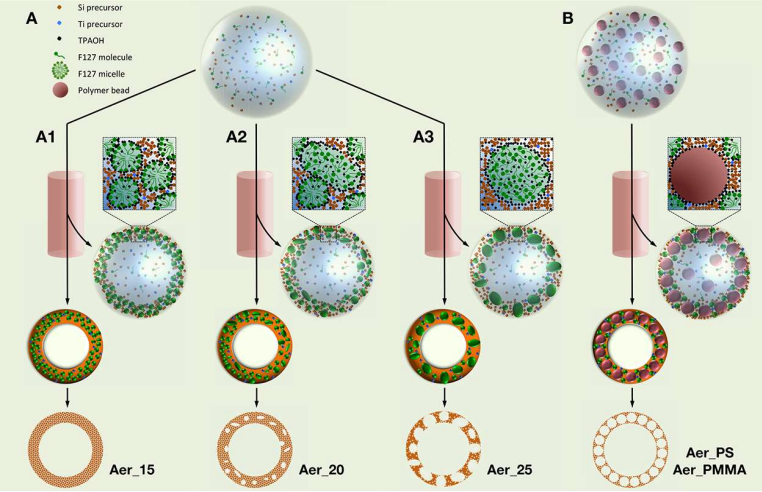

Figure 2. Schematic representation of the routes used for the preparation of TiO_2−SiO_2 with tailored porosity. In "Route A", the porosity was controlled by increasing TPAOH to (Si + Ti) molar ratio, which allows to move from a mesoporous material formed by an EISA mechanism (Route A1) to a macroporous solid resulting from a phase separation mechanism (Routes A2 and A3). In "Route B", macropores were generated by a hard-templating approach using polymer beads of various sizes.

persulfate and sodium dihexylsulfosuccinate according to the procedure of Blas et al.[50] The average particle size measured by dynamic light scattering was 95 nm (fwhm 10 nm).

Aer_PS and **Aer_PMMA** were obtained after mixing 11.17 g of the same precursor solution as **Aer_20** with, respectively, 81 g of PS (7.9% w/w) and 178 g of PMMA (3.6% w/w) latex. The resulting suspension was mixed for 30 min before spray-drying procedure.

A reference **TS-1** catalyst was prepared with a Ti loading of 1.8% by hydrothermal synthesis according to a procedure adapted from the literature,[7] using titanium isopropoxide and TEOS as Ti and Si sources, respectively. The detailed preparation procedure is available in the Supporting Information.

2.2. Characterization of the Materials. The Ti content of the materials was measured by inductively coupled plasma atomic emission spectroscopy (ICP-AES) on an ICP 6500 instrument (Thermo Scientific Instrument) after dissolution of the samples by sodium peroxide fusion. X-ray photoelectron spectroscopy (XPS) experiments were carried out using an SSX 100/206 spectrometer (Surface Science Instruments, USA) with Al Kα radiation operated at 10 kV and 20 mA. The binding energy scale was calibrated on the Si 2p peak, fixed at 103.5 eV.[51] The quantification of Ti in Ti−O−Si and Ti−O−Ti was based on the decomposition of the $2p_{3/2}$ peak at approximately 460.0 and 458.5 eV, respectively.[52,53] Si was quantified on the basis of the Si 2p peak at 103.5 eV.[51] Powder X-ray diffraction (PXRD) patterns were recorded at room temperature on a Siemens D5000 diffractometer equipped with a Ni filter using Cu Kα radiation (Bragg−Brentano geometry) operated at 40 kV and 40 mA. Diffractograms were taken between 5° and 80° (2θ) with a step size of 0.02° (2θ). The band gap energy (E_g) values of **Aer_15** and **Aer_15_2%** were calculated from the optical absorption edge on DR UV−VIS spectra recorded on an Agilent Cary 5000 UV−VIS−NIR spectrophotometer at room temperature in 4000−50 000 cm^{-1} range. The pelletized samples (250−500 μm) were loaded into the U-tube, equipped with a UV−VIS transparent window. Before measurement, the samples were dried at 300 °C under N_2 for 1 h with a heating rate of 5 °C·min^{-1}. After drying, the samples were kept under N_2 during measurement. $BaSO_4$ pellets (250−500 μm), dried according to the same procedure, were used to measure the background spectra. The DR UV−VIS spectra were background corrected and the Kubelka−Munk function was used to display the data. Other spectra were recorded on a Varian Cary 5000 UV−Vis−NIR spectrophotometer with a Harrick single-beam Praying Mantis diffuse reflectance collection system. The spectra were recorded at room temperature in the 12 500−50 000 cm^{-1} range. Spectralon diffuse reflectance standard was used to measure the background spectra. The DR UV−VIS spectra were background corrected and the Kubelka−Munk function was used to display the data. Scanning electron microscopy (SEM) images were taken using a JEOL 7600F microscope at 15 kV voltage. Samples were pretreated with a chromium sputter-coating of 15 nm carried out under vacuum with Sputter Metal 208 HR (Cressington). SEM-field emission gun (FEG) pictures were obtained with Hitachi SU-70. Textural properties were determined from N_2 adsorption/desorption isotherms at −196 °C using a Tristar 3000 instrument (Micromeritics, USA). Prior to measurement, the samples were first degassed overnight under vacuum at 150 °C. The pore size distribution (PSD) was obtained from the adsorption branch using the Barrett−Joyner−Halenda (BJH) method. The specific surface area was evaluated by the Brunauer−Emmett−Teller (BET) method in the relative pressure range of 0.01−0.1 for the aerosol catalysts and 0.01−0.05 for **TS-1**, in order to take into account the presence of micropores.[54] The micropore volume and micropore specific surface area were evaluated by the *t*-plot method in the thickness range of 3.5−5.0 Å.

2.3. Catalytic Activity. The catalytic properties were investigated for the epoxidation of cyclohexene with cumene hydroperoxide (CHP) as the oxidizing agent. The reaction was carried out in a two-necked glass round-bottomed reactor at 90 °C, equipped with a condenser, a magnetic stirrer, and a rubber septum. In a typical run, 0.747 g (0.9 mol·L^{-1}) of cyclohexene (Sigma-Aldrich, 99%), 0.065 g (0.05 mol·L^{-1}) of nonane (TCI, >98%)—used as the internal standard—and 50 mg (5 g·L^{-1}) of the catalyst were premixed in 7.487 g of water-saturated toluene (ca. 330 ppm H_2O) under stirring. After 10 min, 0.342 g (0.18 mol·L^{-1}) of CHP (Sigma, 80%) was added and the mixture was allowed to react for 3 h. The product formation was followed by collecting aliquots at regular time intervals and by analyzing them using gas chromatography, using a Varian CP-3800 chromatograph equipped with a flame ionization detector (FID) and a capillary column (BR-5, 30 m, 0.32 mm i.d., and 1.0 μm film thickness). Catalyst recyclability has been assessed on four consecutive measurements on the same catalyst powder. After each catalytic test, the catalyst was recovered by centrifugation, dried overnight at 120 °C under vacuum, and calcined at 550 °C for 5 h (5 °C/min). The hot filtration test was carried out by removing the catalyst by centrifugation and filtration after 30 min reaction time; the filtrated reaction mixture was then allowed to react for an additional 2 h 30 min.

3. RESULTS AND DISCUSSION

3.1. Preparation of the Materials. The aerosol process[41] consists in atomizing a precursor solution, containing the gel precursors, into small droplets which are dispersed inside a carrier gas (i.e., aerosol) and processed by passing through a heated zone (Figure 1b). In these conditions, the solvent evaporates and the gel quickly condenses and dries, forming solid microspheres. In typical conditions (see the Experimental Section), we expected the formation of spherical particles with a hollow morphology (Figure 1c). The titanium loading was set at 4% in all experiments, which is considerably higher than that in typical TS-1.

Macroporosity and mesoporosity were designed by the use of two types of templating agents (Figure 2): (i) Pluronic F127, a block copolymer surfactant that forms micelles via EISA[55] and (ii) stable colloidal suspensions of PS or PMMA polymer beads. The use of TPAOH ensures the hydrolysis of the titanium precursor and favors Ti^{4+} incorporation in tetrahedral sites. Concomitantly, micropores were also formed in all materials because of the incorporation of TPA^+ cations in the inorganic framework. Although these micropores are not relevant for the conversion of large molecules, their presence demonstrates how we can easily tune the porosity and obtain hierarchically porous materials.

Route A (Figure 2) corresponds to the use of F127 surfactant molecules and TPAOH as templating agents. During aerosol processing, the gel precursors condensed around the self-assembled micelles of the surfactant, which are known to form spherical mesopores of about 6 nm in diameter.[56] However, in addition to the role of a microstructuring agent of TPAOH, it was previously reported that TPA^+ cations are partitioned between the inorganic walls and the F127 micelles, where it plays a role of a swelling agent (at low amount) and a phase-separating agent (at high amount).[44] We thus expected the formation of large mesopores above 6 nm from its use. As a consequence, in the first preparation, we used a F127 to Si molar ratio of 0.005 and a TPAOH to (Si + Ti) molar ratio of 0.15 to prepare a dual micro−mesostructured material (Route A1, Figure 2). After calcination, to remove the organics and release the porosity, the material was denoted as "**Aer_15**".

Variation of the TPAOH amount can be used to tune the pore size of mixed oxides, as it was recently reported for the preparation of aluminosilicate acid catalysts with large pores.[44] By increasing the TPAOH to (Si + Ti) molar ratio in the precursor solution to 0.20 and 0.25 (respectively, Route A2 and Route A3, Figure 2), the pH increased and the condensation rate of the precursors decreased. Besides, the swelling effect of TPA^+ was amplified as more cations were incorporated in the organic phase. In these conditions, a phase separation was initiated because the interactions between the organic and inorganic phases became too low to stabilize the mesostructure by EISA.[44,57] In the typical conditions of spray-dry processing, this metastable system has been quenched before it reached the thermodynamic equilibrium, corresponding to a complete phase separation.[58] Using a TPAOH to (Si + Ti) molar ratio of 0.20, we obtained a material with a heterogeneous porosity resulting from the early transition between EISA and phase separation. This material was denoted as "**Aer_20**". When the amount of TPAOH was the highest [i.e., TPAOH/(Si + Ti) = 0.25], the material, denoted as "**Aer_25**", almost presented a dual micro−macroporosity, with only a small proportion of mesopores in the material (see Figure 2 and textural analysis below).

Although this strategy is appealing to tailor the porosity at micro-, meso-, and macroscales, the control over the macroporosity is not straightforward whenever phase separation is involved; for instance, the temperature gradient in the heating part of the spray-drying apparatus may produce variable drying time and thus large macroPSDs. Therefore, in Route B (Figure 2), PS (95 ± 10 nm fwhm) or PMMA (278 ± 63 nm fwhm) polymer beads were used as hard templates[59] to prepare alternative and well-controlled porous materials with a three-level micro−meso−macrostructure.[49,50] The latex were thoroughly mixed with the same precursor solution as **Aer_20** and spray-dried at 75 °C, thus lower than the glass transition temperature of the polymers (ca. 100 °C for PS and ca. 105 °C for PMMA). The final composition of the precursor solution allowed the incorporation of the polymer beads in a close-packing arrangement. The materials were named "**Aer_PS**" and "**Aer_PMMA**".

3.2. Characterization of the Materials. Elemental analysis (Table 1) showed that the experimental bulk Ti content was close to the nominal content for all catalysts. This result demonstrates an excellent control over the bulk composition, with a quantitative incorporation of both titanium and silicon species in the final material.

Table 1. Percentage of Ti Species (mol Ti/(mol Ti + mol Si) × 100%) in the Catalysts (Bulk Composition, ICP-AES) and at the Catalysts Surface (from XPS)

	bulk Ti %[a]	surf. Ti %	surf. Ti−O−Si %	% Ti−O−Si[b]
TS-1	1.6 (1.8)	1.3	1.2	90
Aer_15	4.0 (4.0)	3.3	2.8	85
Aer_20	4.8 (4.0)	4.2	3.5	85
Aer_25	4.7 (4.0)	4.3	3.6	84
Aer_PS	4.5 (4.0)	3.8	3.3	85
Aer_PMMA	4.5 (4.0)	3.5	3.0	84

[a]Nominal composition (corresponding to the precursor solution) is given in brackets. [b]% Ti−O−Si = (surf. Ti−O−Si %/surf. Ti %) × 100.

XPS analyses were conducted in order to investigate the surface composition and the quality of the Ti dispersion at the surface (Table 1, see also Figure S1, Supporting Information). For all aerosol catalysts, the surface Ti concentration is close to the bulk content, showing that the aerosol method leads to homogeneous mixed oxide particle compositions, as there is no relative enrichment of the surface with Si or Ti oxide.

Among Ti detected at the surface of the catalyst by XPS, one can distinguish the fraction which is truly incorporated into the silica matrix (denoted as "Ti−O−Si" in Table 1) from the fraction which is not dispersed and is instead present as extraframework Ti−O−Ti species. The former is found at ca. 460.0 eV and the latter is found at ca. 458.5 eV.[52,53] The Ti 2p peak deconvolution is shown in Figure S1 for all catalysts. In TS-1, it is well known that almost all surface Ti atoms are incorporated in the well-defined crystalline framework. Indeed, the results show a proportion of well-dispersed surface Ti atoms of 90% for this sample. These isolated Ti sites are known to be the active epoxidation species.[4,5] Importantly, aerosol-made catalysts show a similar excellent dispersion (Table 1). Moreover, the absolute amount of dispersed Ti−

O−Si at the surface is twice as high as for **TS-1**, in line with the corresponding higher Ti loading (viz ∼4 vs 1.8%).

PXRD analyses indicated that the aerosol catalysts are all amorphous (Figure S2, Supporting Information). No evidence of the presence of a TiO_2 crystalline phase, such as anatase with characteristic reflection at $2\theta = 25°$, was found, which excludes the presence of TiO_2 crystallites larger than 5 nm. The **TS-1** reference catalyst showed the expected diffraction pattern, typical for its MFI structure.[7]

The high dispersion of Ti in aerosol catalysts is further confirmed by the maximum absorption band in the 215−225 nm range on the DRUV−vis spectra of the catalysts, which corresponds to Ti atoms in tetrahedral coordination (Figure 3).[60] The small contribution above 250 nm could be

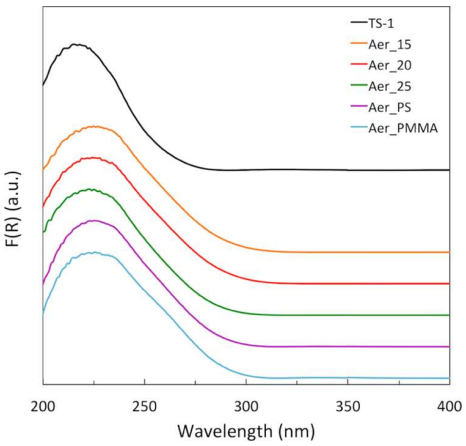

Figure 3. DRS UV−visible spectra of the catalysts (Kubelka−Munk Function).

characteristic of the presence of small amounts of Ti in higher coordination number, for instance, because of water coordination, local oligomeric Ti species, or small TiO_2 nanodomains.[60−62] However, no evidence of the presence of a crystalline phase such as anatase, having maximum characteristic absorption around 330 nm,[63] could be found in the spectra.

SEM and SEM-FEG images of the mixed oxides are shown in Figure 4 (route A) and Figure 5 (route B). The TiO_2−SiO_2 microspheres are in the 1−20 μm size range and mainly show a hollow spherical structure with some distortion. Images in

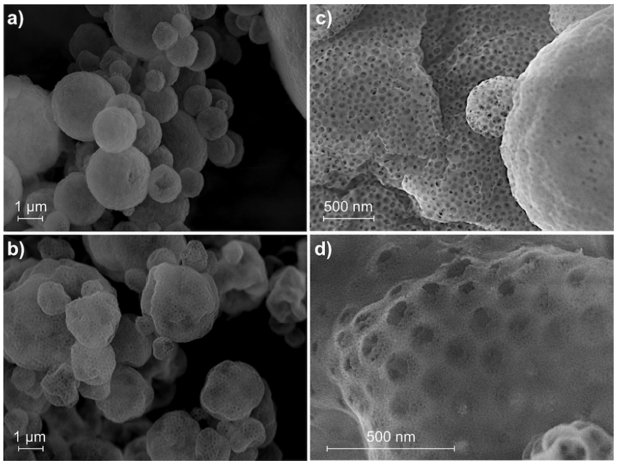

Figure 5. SEM (a,b) and SEM-FEG (c,d) images of **Aer_PS** (a,c) and **Aer_PMMA** (b,d). Additional SEM-FEG images can be found in the Supporting Information (Figure S3).

Figure 4 unravel the effect of the amount of TPAOH on the pore size. **Aer_15** shows a regular porous structure with small mesopores clearly visible in the SEM-FEG image (Figure 4d). **Aer_20** presents the same type of pores at the external surface, but also shows the characteristic structure of an early stage phase separation, with discernible large pores formed mainly on the inner side of the shell (Figure 4e). By comparison, **Aer_25** reached a more advanced state of phase separation which strongly affected the mesostructuration of the material. For this catalyst, macropores as large as 200 nm are clearly distinguishable at the surface (Figure 4c,f).

Alternatively, macropores have been formed using polymer beads as a sacrificial template. The same kind of distorted hollow structures is observed (Figure 5). SEM-FEG confirms that the beads, which were removed by calcination, were in a close-packing arrangement during the formation of the solid. The macropore dimensions are ca. 80 nm and 150−200 nm for **Aer_PS** and **Aer_PMMA**, respectively, in line with the template size. The small shrinkage of the macropores observed for **Aer_PMMA** may be attributed to partial hydrolysis of the PMMA side chains into polyacrylic acid under basic conditions.[64]

N_2-physisorption isotherms are shown in Figure 6, along with the BJH PSDs. The presence of mesopores in all aerosol samples is evidenced by the type IV isotherms, which are

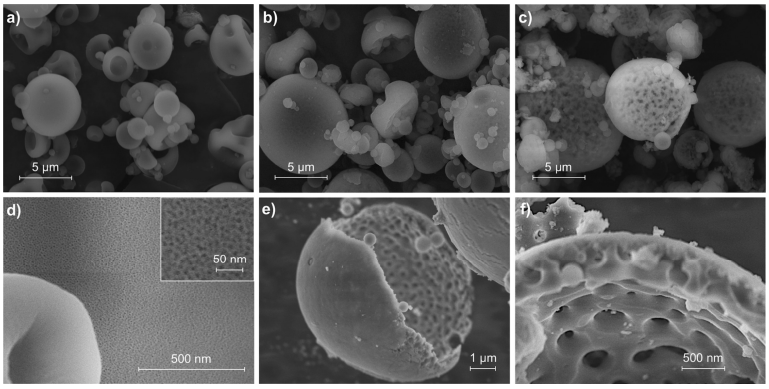

Figure 4. SEM (a−c) and SEM-FEG (d−f) images of **Aer_15** (a,d), **Aer_20** (b,e), and **Aer_25** (c,f).

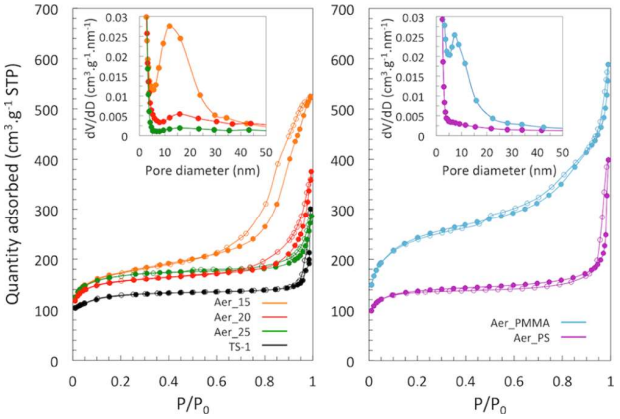

Figure 6. N_2 adsorption–desorption isotherms of the TiO_2–SiO_2 mixed oxides prepared by aerosol with different templates: the F127 surfactant with various TPAOH to (Si + Ti) molar ratios (left) and PS and PMMA polymer beads (right). PSDs based on the adsorption branch are shown in the inset. The isotherm of microporous **TS-1** is shown for comparison. Full symbols are used for the adsorption isotherms and empty symbols are used for the desorption isotherms.

typically observed for mesoporous solids. Textural data are summarized in Table 2. As expected, **TS-1** solely displayed

Table 2. Textural Properties of the Aerosol Catalysts Compared to the Reference Material TS-1

	S_{BET} ($m^2 \cdot g^{-1}$)[a]	S_μ ($m^2 \cdot g^{-1}$)[b]	V_p ($cm^3 \cdot g^{-1}$)[c]	V_μ ($cm^3 \cdot g^{-1}$)[b]
TS-1	510	380	0.43	0.15
Aer_15	640	380	0.79	0.16
Aer_20	630	450	0.48	0.18
Aer_25	620	450	0.38	0.19
Aer_PS	520	370	0.45	0.15
Aer_PMMA	890	380	0.80	0.15

[a]To take into account the presence of micropores, the BET method was applied in a low P/P_0 range, as proposed by Rouquerol.[54] [b]Micropore specific surface area and micropore volume calculated from the *t*-plot (see Figure S4, Supporting Information). [c]Measured at P/P_0 = 0.98.

micropores and interparticular spaces which contribute to the total pore volume. In comparison, much higher total pore volumes and BET areas were obtained by the aerosol method, whereas the micropore volumes and the micropore specific surface areas were in the same range. Subtracting the microporous component, all aerosol catalysts thus have higher specific surface areas and pore volumes compared to **TS-1** and are therefore expected to facilitate the conversion of large molecules.

PSDs of **Aer_15**, **Aer_20**, and **Aer_25** are centered at ca. 15 nm (inset, Figure 6). This pore size should be related to the formation of swollen F127 micelles, whose diameter has been increased by the incorporation of TPA^+ cations.[44] By increasing the TPAOH amount, this swelling effect is amplified and leads to the disruption of the micelles, likely explaining a part of the phase separation phenomenon.[57] **Aer_20** and **Aer_25** therefore present a lower mesostructuration, as evidenced by the shape of the isotherms (Figure 6). Nevertheless, the BET areas remain comparable (Table 2).

Aer_PS and **Aer_PMMA** appear to have lower micropore volumes (Table 2). This could be explained by strong interactions between the polymer chains and TPA^+ cations, which could tend to adsorb at the surface of the polymer beads and therefore be unavailable to act as the structuring agent (see Route B, Figure 2). For the same reason, the role of TPA^+ cations as a swelling agent is compromised, resulting in lower mesopore size for **Aer_PMMA** (ca. 10 nm). In the case of **Aer_PS**, such mesopores are absent and we assume that the close packing of the PS beads creates inorganic walls which are too thin to accommodate the F127 micelles. It must be noted that the BET area of **Aer_PMMA** is comparatively high (890 $m^2 \cdot g^{-1}$); this appears to be because of the presence of additional mesopores smaller than 3.8 nm. Although not appearing clearly on the adsorption branch PSD (inset, Figure 6), these pores can be evidenced by the forced closure of the isotherm upon desorption at the P/P_0 value of 0.4–0.5 because of the tensile strength effect, and visualized on the desorption branch PSD (see Figure S5, Supporting Information).[65] These small mesopores may result from the interpenetration of linear polymer chains within the inorganic phase.

3.3. Catalytic Performance. The materials were tested in the batch mode for the epoxidation of cyclohexene, which is commonly used as a model substrate for the epoxidation of bulky olefins. Using hydrogen peroxide (30% w/w aqueous solution) as the oxidant, the aerosol catalysts showed much higher epoxidation activity as compared to **TS-1** (Figure S6 and Table S1). Yet, we observed a ca. 60% activity loss after four consecutive tests carried out on the **Aer_20** catalyst, whereas **TS-1** kept the same activity (Figure S7). In fact, it is generally accepted that amorphous catalysts—such as Ti supported on MCM-41[66] or SBA-15[67] as well as TiO_2–SiO_2 mixed oxides[68]—are sensitive to water[69] and therefore encounter activity and selectivity issues when aqueous H_2O_2 is used as the oxidant. This constitutes a certain limitation to our aerosol-made catalysts.

Thus, the epoxidation of cyclohexene was investigated in organic conditions, using CHP as the oxidant because it has been shown to lead to much higher performance for amorphous titanosilicate catalysts,[70,71] including aerogels[72] and xerogels.[73,74] A hot filtration test was carried out, confirming that all the catalytic activity was attributable only to the solid material (see Figure S8).

In addition to the targeted epoxide formation by the direct epoxidation pathway (Path A, Figure 7), the reaction scheme for cyclohexene epoxidation reveals the possible formation of other products, including cyclohexane diol, formed by the epoxide ring-opening, as well as 2-cyclohexen-1-ol and its oxidation product 2-cyclohexen-1-one, formed by an unwanted radical oxidation pathway (Path B, Figure 7).

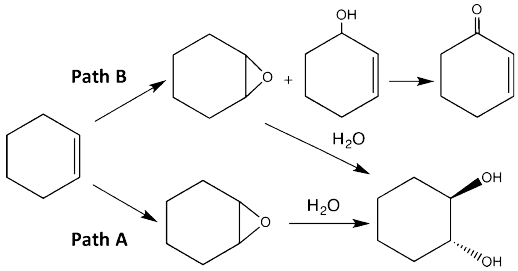

Figure 7. Reaction scheme for the epoxidation of cyclohexene. Path A refers to the direct epoxidation pathway and Path B refers to the radical oxidation pathway.

Under the experimental conditions depicted in Figure 8, our catalysts present a much higher epoxide yield compared to **TS-1**. From Table 3, all aerosol catalysts also present a higher CHP conversion compared to the reference zeolite. Comparison among the catalysts is also presented in terms of initial turnover frequency (TOF), approximated by the CHP conversion at the early stage of the reaction (15 min). All catalysts presented a higher intrinsic activity (TOF) when using CHP as the oxidant, as compared to hydrogen peroxide (Table S1). This is in agreement with results previously reported by Chiker et al. on Ti–SBA-15 catalysts.[71] The selectivity toward the epoxide reaches 88–98% for the aerosol catalysts (Table 3), the remaining gap in product selectivity being mainly explained by the hydrolysis of the epoxide to form cyclohexane diol.

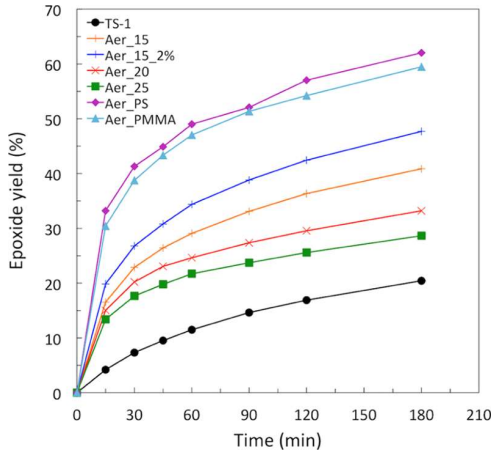

Figure 8. Kinetic data in terms of epoxide yield for the reaction of cyclohexene with CHP in toluene. Experimental conditions: T = 90 °C, [CATA] = 5 g·L^{-1}, [cyclohexene] = 0.9 mol·L^{-1}, and [CHP] = 0.18 mol·L^{-1}.

In the case of **TS-1**, almost no cyclohexane diol is formed, consistent with the fact that the intrinsic hydrophobicity of the zeolite might repel water molecules from the catalyst surface.[5] However, the selectivity toward the epoxide—defined as the amount of epoxide formed divided by the amount of CHP consumed—is found to be higher than 100%. In fact, we found that the same reaction, carried out in the absence of CHP, leads to a production of epoxide and 2-cyclohexen-1-ol in similar amounts. Actually, molecular oxygen was already reported to be able to trigger the radical oxidation pathway (Path B, Figure 7) in the epoxidation of cyclohexene.[75] Therefore, we interpret the unrealistic selectivity value obtained for **TS-1** in the light of a nonselective and CHP-independent formation of the epoxide. This interpretation is further supported by the presence of a significant amount of 2-cyclohexen-1-ol in this case (Table 3). Interestingly, the nonselective oxidation of cyclohexene seems to only occur on **TS-1** because no 2-cyclohexen-1-ol and almost no 2-cyclohexen-1-one are found in the case of the aerosol catalysts, which all appear to operate via the direct epoxidation pathway only (Path A, Figure 7).

The higher catalytic activity obtained with the aerosol catalysts can be ascribed to two key features: (i) the higher amount of well-incorporated Ti at the catalyst surface and (ii) the texture and pore architecture, with a higher specific surface area compared to **TS-1** zeolite associated with the presence of accessible mesopores. To discriminate between these two possible explanations, we synthesized an aerosol catalyst with a nominal Ti loading of 2% (bulk)—closer to that of **TS-1**—while keeping the same gel composition as **Aer_15** ("**Aer_15_2%**"). In terms of texture, this catalyst was very similar to **Aer_15**, with a BET area of 790 m^2·g^{-1}, a pore volume of 0.87 cm^3·g^{-1}, and a similar PSD (see Figure S9). The experimental surface Ti–O–Si content determined by XPS was 1.3%, similar to **TS-1** (1.2%). **Aer_15_2%** had an initial TOF about three times higher when compared to **TS-1** (Table 3). This is a strong indication of the positive impact of the hierarchical texture of the aerosol catalyst on the activity, allowing faster molecular transport through the catalyst. Interestingly, the overall yield and selectivity of **Aer_15_2%** is similar to that of **Aer_15**, despite a two times lower Ti content and comparable texture. This translates into more than twofold higher initial TOF for **Aer_15_2%**. Calculating the band gap energy (E_g) of the catalysts from the optical absorption edges in the DR UV–vis spectra obtained in dehydrated conditions[76−78] (see Figure S10), we found that the value of E_g for **Aer_15_2%** (4.75 eV) is higher than that for **Aer_15** (4.50 eV). The higher E_g value of **Aer_15_2%** is related to a relatively higher proportion of isolated tetrahedral Ti species, which contributes to the increase in the epoxidation rate per surface Ti site.

The catalysts prepared by aerosol, having the same Ti loading and similar Ti speciation, reached different levels of

Table 3. Yield (Y), Conversion (X), Selectivity (S), and Initial TOF for Ti-Catalyzed Cyclohexene Epoxidation at 90 °C (3 h) with Cumene Hydroperoxide

	Y_{Epox} (%)[a]	Y_{Diol} (%)[a]	$Y_{Alcohol}$ (%)[a]	Y_{Ketone} (%)[a]	X_{CHP} (%)	S_{Epox} (%)	PB S_{Epox} (%)[b]	TOF (h^{-1})[c]
TS-1	20	<1	3	0	16	126	87	38
Aer_15	41	2	0	<1	46	89	94	49
Aer_15_2%	48	2	0	<1	52	92	96	125
Aer_20	33	2	0	<1	37	91	94	37
Aer_25	29	2	0	<1	31	92	93	30
Aer_PS	62	1	0	<1	63	98	97	92
Aer_PMMA	59	3	0	<1	67	88	95	85

[a]Yields are expressed as the amount of the product formed divided by the initial amount of CHP. Epox = cyclohexene oxide, diol = cyclohexane diol, alcohol = 2-cyclohexen-1-ol, and ketone = 2-cyclohexen-1-one. [b]Product-based selectivity; these values have been calculated by dividing the epoxide yield by the overall yield instead of the CHP conversion. [c]Initial TOF approximated from the CHP conversion at 15 min reaction time. It is defined as the number of mole of CHP converted per minute divided by the number of active sites (deduced from "surf. Ti–O–Si %", Table 1); one example of TOF calculation is shown in the Supporting Information.

activity. This is tentatively correlated with their textural properties. For **Aer_25**, **Aer_20**, and **Aer_15**, the activity tends to increase as the specific surface area increases and as the microporous specific surface area decreases, pointing to a possible beneficial effect of increasing the accessible surface area. The much higher performance reached by **Aer_PS** and **Aer_PMMA** does not seem to be fully explained by a high accessible surface area. Although this should be verified by dedicated experiments on diffusion phenomena, we suggest that the macroporosity created by the close packing of polymer beads facilitates mass transport phenomena, owing to the thinness of the walls that separate the macropores.[79]

A recyclability study carried out on **Aer_20** revealed that there was only a ca. 20% decrease of the catalytic activity over four consecutive tests (Figure 9), much less than for the same

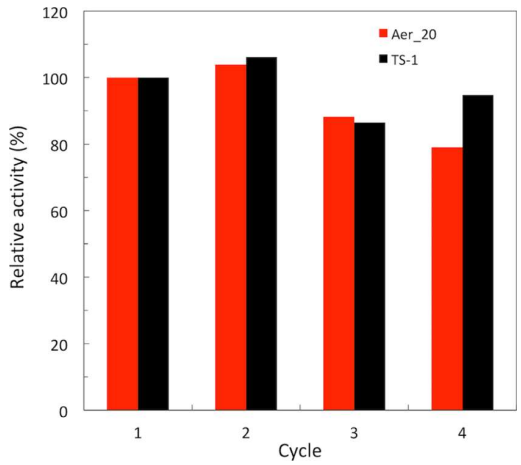

Figure 9. Recyclability study of the **TS-1** and **Aer_20** catalysts with CHP as the oxidant. Data were collected in the initial stage of the reaction (15 min reaction time), and the catalytic activity (expressed in terms of CHP conversion) relative to the first test was calculated for each catalyst. The composition was identical to Figure 8.

catalyst tested in the presence of aqueous solution of H_2O_2. This small decrease could be associated to the presence of small amounts of water in the solvent and potentially could be further improved by working under strict nonaqueous conditions.[28] Also, a N_2 physisorption analysis carried out on **Aer_20** and **TS-1** after the four consecutive cycles revealed a ca. 25% decrease of the BET area and pore volume for the aerosol catalyst (490 $m^2 \cdot g^{-1}$, 0.37 $cm^3 \cdot g^{-1}$), whereas the BET area and pore volume of **TS-1** were not affected (550 $m^2 \cdot g^{-1}$, 0.40 $cm^3 \cdot g^{-1}$). This result suggests that the decrease in activity for the aerosol catalyst may also be due to a surface loss upon repetitive reaction cycles and could be avoided by optimizing the recycling procedure.

4. CONCLUSIONS

In this paper, we demonstrated that the aerosol technique is a powerful technology for the preparation of TiO_2–SiO_2 mixed oxides possessing a variety of pore sizes and architectures, while controlling simultaneously the composition, homogeneity, and dispersion of the titanium species. High specific surface areas with large pores in the meso- and macroporous range were reached. These latter characteristics stand for the higher catalytic performance of these materials for the epoxidation of cyclohexene compared to TS-1. Though these materials can accommodate a higher Ti loading than typical TS-1 zeolite, the increasing titanium loading was shown not to lead to a substantial increase of the epoxidation performance (TOF), as it results in higher Ti coordination.

TiO_2–SiO_2 catalysts prepared by aerosol processing have a high potential for the synthesis of bulkier and highly valuable epoxides (e.g., α-pinene oxide, norbonene oxide, and linalool oxide) potentially in the continuous flow mode because the particle size should permit the design of a fixed bed reactor. Besides, it should be reminded that such an aerosol process can easily be scaled-up, thus meeting requirements for future industrial applications.

■ ACKNOWLEDGMENTS

Authors acknowledge the "Communauté française de Belgique" for the financial support through the ARC programme (15/20-069). F. Devred is acknowledged for the technical and logistical support. V.S. is thankful to F.R.S.–F.N.R.S for his FRIA PhD grant. The authors thank the Francqui Foundation for the chair, which made it possible for Prof. Sanchez to visit Belgium. FEGSEM instrumentation was facilitated by the Institut des Matériaux de Paris Centre (IMPC FR2482) and was funded by UPMC, CNRS, and the C'Nano projects of the Région Ile-de-France. Elise Peeters acknowledges funding by an FWO SB fellowship. M.D. thanks Research Foundation - Flanders (FWO) for funding.

■ REFERENCES

(1) Taramasso, M.; Perego, G.; Notari, B. Preparation of Porous Crystalline Synthetic Material Comprised of Silicon and Titanium Oxides. U.S. Patent 4,410,501 A, Oct 18, 1983.

(2) Perego, C.; Carati, A.; Ingallina, P.; Mantegazza, M. A.; Bellussi, G. Production of Titanium Containing Molecular Sieves and Their Application in Catalysis. *Appl. Catal., A* **2001**, *221*, 63–72.

(3) Fisher, W. B.; Crescentini, L.; Staff, U. *Kirk–Othmer Encyclopedia of Chemical Technology*; American Cancer Society, 2015; pp 1–11.
(4) Clerici, M. G.; Ingallina, P. Epoxidation of Lower Olefins with Hydrogen Peroxide and Titanium Silicalite. *J. Catal.* **1993**, *140*, 71–83.
(5) Clerici, M. G. The Activity of Titanium Silicalite-1 (TS-1): Some Considerations on Its Origin. *Kinet. Catal.* **2015**, *56*, 450–455.
(6) Millini, R.; Previde Massara, E.; Perego, G.; Bellussi, G. Framework Composition of Titanium Silicalite-1. *J. Catal.* **1992**, *137*, 497–503.
(7) Thangaraj, A.; Eapen, M. J.; Sivasanker, S.; Ratnasamy, P. Studies on the Synthesis of Titanium Silicalite, TS-1. *Zeolites* **1992**, *12*, 943–950.
(8) Murugavel, R.; Roesky, H. W. Titanosilicates: Recent Developments in Synthesis and Use as Oxidation Catalysts. *Angew. Chem., Int. Ed.* **1997**, *36*, 477–479.
(9) Přech, J. Catalytic Performance of Advanced Titanosilicate Selective Oxidation Catalysts – a Review. *Catal. Rev.: Sci. Eng.* **2018**, *60*, 71–131.
(10) Zuo, Y.; Liu, M.; Zhang, T.; Meng, C.; Guo, X.; Song, C. Enhanced Catalytic Performance of Titanium Silicalite-1 in Tuning the Crystal Size in the Range 1200-200 nm in a Tetrapropylammonium Bromide System. *ChemCatChem* **2015**, *7*, 2660–2668.
(11) Liu, H.; Lu, G.; Guo, Y.; Guo, Y.; Wang, J. Deactivation and Regeneration of TS-1/Diatomite Catalyst for Hydroxylation of Phenol in Fixed-Bed Reactor. *Chem. Eng. J.* **2005**, *108*, 187–192.
(12) Guo, Z.; Xiong, G.; Liu, L.; Li, P.; Hao, L.; Cao, Y.; Tian, F. Aerosol-Assisted Synthesis of Hierarchical Porous Titanosilicate Molecular Sieve as Catalysts for Cyclohexene Epoxidation. *J. Porous Mater.* **2015**, *23*, 407–413.
(13) Na, K.; Jo, C.; Kim, J.; Ahn, W.-S.; Ryoo, R. MFI Titanosilicate Nanosheets with Single-Unit-Cell Thickness as an Oxidation Catalyst Using Peroxides. *ACS Catal.* **2011**, *1*, 901–907.
(14) Přech, J.; Eliášová, P.; Aldhayan, D.; Kubů, M. Epoxidation of Bulky Organic Molecules over Pillared Titanosilicates. *Catal. Today* **2015**, *243*, 134–140.
(15) Stark, W. J.; Pratsinis, S. E.; Baiker, A. Flame Made Titania/Silica Epoxidation Catalysts. *J. Catal.* **2001**, *203*, 516–524.
(16) Grunwaldt, J.-D.; Beck, C.; Stark, W.; Hagen, A.; Baiker, A. In situ XANES study on TiO_2-SiO_2 aerogels and flame made materials. *Phys. Chem. Chem. Phys.* **2002**, *4*, 3514–3521.
(17) Stark, W. J.; Kammler, H. K.; Strobel, R.; Günther, D.; Baiker, A.; Pratsinis, S. E. Flame-Made Titania/Silica Epoxidation Catalysts: Toward Large-Scale Production. *Ind. Eng. Chem. Res.* **2002**, *41*, 4921–4927.
(18) Corma, A. From Microporous to Mesoporous Molecular Sieve Materials and Their Use in Catalysis. *Chem. Rev.* **1997**, *97*, 2373–2420.
(19) Vansant, E. F. Pore Size Engineering in Zeolites. In *Studies in Surface Science and Catalysis*; Grobet, P. J., Mortier, W. J., Vansant, E. F., Schulz-Ekloff, G., Eds.; Innovation in Zeolite Materials Science; Elsevier, 1988; Vol. 37, pp 143–153.
(20) Camblor, M. A.; Corma, A.; Martínez, A.; Pérez-Pariente, J. Synthesis of a Titaniumsilicoaluminate Isomorphous to Zeolite Beta and Its Application as a Catalyst for the Selective Oxidation of Large Organic Molecules. *J. Chem. Soc., Chem. Commun.* **1992**, 589–590.
(21) Blasco, T.; Corma, A.; Navarro, M. T.; Pariente, J. P. Synthesis, Characterization, and Catalytic Activity of Ti-MCM-41 Structures. *J. Catal.* **1995**, *156*, 65–74.
(22) Smeets, V.; van den Biggelaar, L.; Barakat, T.; Gaigneaux, E. M.; Debecker, D. P. Macrocellular Titanosilicate. *ChemRxiv* **2019**, DOI: 10.26434/chemrxiv.7578599.v1.
(23) Hutter, R.; Mallat, T.; Baiker, A. Titania Silica Mixed Oxides. *J. Catal.* **1995**, *153*, 177–189.
(24) Dutoit, D. C. M.; Schneider, M.; Baiker, A. Titania aerogels prepared by low-temperature supercritical drying. Influence of extraction conditions. *J. Catal.* **1995**, *1*, 165–174.
(25) Smeets, V.; Ben Mustapha, L.; Schnee, J.; Gaigneaux, E. M.; Debecker, D. P. Mesoporous SiO_2-TiO_2 Epoxidation Catalysts: Tuning Surface Polarity to Improve Performance in the Presence of Water. *Mol. Catal.* **2018**, *452*, 123–128.
(26) Lafond, V.; Mutin, P. H.; Vioux, A. Control of the Texture of Titania–Silica Mixed Oxides Prepared by Nonhydrolytic Sol–Gel. *Chem. Mater.* **2004**, *16*, 5380–5386.
(27) Cojocariu, A. M.; Mutin, P. H.; Dumitriu, E.; Fajula, F.; Vioux, A.; Hulea, V. Mild oxidation of bulky organic compounds with hydrogen peroxide over mesoporous TiO_2-SiO_2 xerogels prepared by non-hydrolytic sol-gel. *Appl. Catal., B* **2010**, *97*, 407–413.
(28) Lorret, O.; Lafond, V.; Mutin, P. H.; Vioux, A. One-Step Synthesis of Mesoporous Hybrid Titania–Silica Xerogels for the Epoxidation of Alkenes. *Chem. Mater.* **2006**, *18*, 4707–4709.
(29) Brinker, C. J.; Scherer, G. W. *Sol–Gel Science: The Physics and Chemistry of Sol–Gel Processing*; Academic Press, 2013.
(30) Livage, J.; Sanchez, C. Sol-Gel Chemistry. *J. Non-Cryst. Solids* **1992**, *145*, 11–19.
(31) Debecker, D. P. Innovative Sol-Gel Routes for the Bottom-up Preparation of Heterogeneous Catalysts. *Chem. Rec.* **2018**, *18*, 662–675.
(32) Landau, M. V. Sol–Gel Process. *Handbook of Heterogeneous Catalysis*; American Cancer Society, 2008; pp 119–160.
(33) Brinker, C. J.; Lu, Y.; Sellinger, A.; Fan, H. Evaporation-Induced Self-Assembly: Nanostructures Made Easy. *Adv. Mater.* **1999**, *11*, 579–585.
(34) Zhong, R.; Peng, L.; de Clippel, F.; Gommes, C.; Goderis, B.; Ke, X.; Van Tendeloo, G.; Jacobs, P. A.; Sels, B. F. An Eco-Friendly Soft Template Synthesis of Mesostructured Silica-Carbon Nanocomposites for Acid Catalysis. *ChemCatChem* **2015**, *7*, 3047–3058.
(35) Schneider, M.; Baiker, A. Aerogels in Catalysis. *Catal. Rev.: Sci. Eng.* **1995**, *37*, 515–556.
(36) Livage, J.; Henry, M.; Sanchez, C. Sol-Gel Chemistry of Transition Metal Oxides. *Prog. Solid State Chem.* **1988**, *18*, 259–341.
(37) Sanchez, C.; Livage, J.; Henry, M.; Babonneau, F. Chemical Modification of Alkoxide Precursors. *J. Non-Cryst. Solids* **1988**, *100*, 65–76.
(38) Debecker, D. P.; Mutin, P. H. Non-hydrolytic sol-gel routes to heterogeneous catalysts. *Chem. Soc. Rev.* **2012**, *41*, 3624–3650.
(39) Boissiere, C.; Grosso, D.; Chaumonnot, A.; Nicole, L.; Sanchez, C. Aerosol Route to Functional Nanostructured Inorganic and Hybrid Porous Materials. *Adv. Mater.* **2010**, *23*, 599–623.
(40) Nandiyanto, A. B. D.; Okuyama, K. Progress in Developing Spray-Drying Methods for the Production of Controlled Morphology Particles: From the Nanometer to Submicrometer Size Ranges. *Adv. Powder Technol.* **2011**, *22*, 1–19.
(41) Debecker, D. P.; Le Bras, S.; Boissière, C.; Chaumonnot, A.; Sanchez, C. Aerosol Processing: A Wind of Innovation in the Field of Advanced Heterogeneous Catalysts. *Chem. Soc. Rev.* **2018**, *47*, 4112–4155.
(42) Maksasithorn, S.; Praserthdam, P.; Suriye, K.; Debecker, D. P., Preparation of super-microporous WO_3-SiO_2 olefin metathesis catalysts by the aerosol-assisted sol-gel process. *Microporous Mesoporous Mater.* **2015**, *213*, 125–133.
(43) Debecker, D. P.; Stoyanova, M.; Colbeau-Justin, F.; Rodemerck, U.; Boissière, C.; Gaigneaux, E. M.; Sanchez, C. One-Pot Aerosol Route to MoO_3-SiO_2-Al_2O_3 Catalysts with Ordered Super Microporosity and High Olefin Metathesis Activity. *Angew. Chem., Int. Ed.* **2012**, *51*, 2129–2131.
(44) Pega, S.; Boissière, C.; Grosso, D.; Azaïs, T.; Chaumonnot, A.; Sanchez, C. Direct Aerosol Synthesis of Large-Pore Amorphous Mesostructured Aluminosilicates with Superior Acid-Catalytic Properties. *Angew. Chem., Int. Ed.* **2009**, *48*, 2784–2787.
(45) Wang, C. Y.; Bai, H. Aerosol Processing of Mesoporous Silica Supported Bimetallic Catalysts for Low Temperature Acetone Oxidation. *Catal. Today* **2011**, *174*, 70–78.
(46) Jung, K. Y.; Jung, Y. R.; Jeon, J.-K.; Kim, J. H.; Park, Y.-K.; Kim, S. Preparation of Mesoporous V_2O_5/TiO_2 via Spray Pyrolysis and Its

Application to the Catalytic Conversion of 1, 2-Dichlorobenzene. *J. Ind. Eng. Chem.* **2011**, *17*, 144−148.
(47) Vivian, A.; Fusaro, L.; Debecker, D. P.; Aprile, C. Mesoporous Methyl-Functionalized Sn-Silicates Generated by the Aerosol Process for the Sustainable Production of Ethyl Lactate. *ACS Sustainable Chem. Eng.* **2018**, *6*, 14095−14103.
(48) Sachse, A.; Hulea, V.; Kostov, K. L.; Marcotte, N.; Boltoeva, M. Y.; Belamie, E.; Alonso, B. Efficient mesoporous silica-titania catalysts from colloidal self-assembly. *Chem. Commun.* **2012**, *48*, 10648−10650.
(49) Goodwin, J. W.; Hearn, J.; Ho, C. C.; Ottewill, R. H. Studies on the preparation and characterisation of monodisperse polystyrene laticee. *Colloid Polym. Sci.* **1974**, *252*, 464−471.
(50) Blas, H.; Save, M.; Pasetto, P.; Boissiére, C.; Sanchez, C.; Charleux, B. Elaboration of Monodisperse Spherical Hollow Particles with Ordered Mesoporous Silica Shells via Dual Latex/Surfactant Templating: Radial Orientation of Mesopore Channels. *Langmuir* **2008**, *24*, 13132−13137.
(51) Jacquemin, M.; Genet, M. J.; Gaigneaux, E. M.; Debecker, D. P. Calibration of the X-Ray Photoelectron Spectroscopy Binding Energy Scale for the Characterization of Heterogeneous Catalysts: Is Everything Really under Control? *ChemPhysChem* **2013**, *14*, 3618−3626.
(52) Erdem, B.; Hunsicker, R. A.; Simmons, G. W.; Sudol, E. D.; Dimonie, V. L.; El-Aasser, M. S. XPS and FTIR Surface Characterization of TiO_2 Particles Used in Polymer Encapsulation. *Langmuir* **2001**, *17*, 2664−2669.
(53) Reddy, B. M.; Chowdhury, B.; Smirniotis, P. G. An XPS study of the dispersion of MoO_3 on TiO_2-ZrO_2, TiO_2-SiO_2, TiO_2-Al_2O_3, SiO_2-ZrO_2, and SiO_2-TiO_2-ZrO_2 mixed oxides. *Appl. Catal., A* **2001**, *211*, 19−30.
(54) Rouquerol, J.; Llewellyn, P.; Rouquerol, F. Is the Bet Equation Applicable to Microporous Adsorbents? In *Studies in Surface Science and Catalysis*; Llewellyn, P. L., Rodriquez-Reinoso, F., Rouqerol, J., Seaton, N., Eds.; Characterization of Porous Solids VII; Elsevier, 2007; Vol. *160*, pp 49−56.
(55) Lu, Y.; Fan, H.; Stump, A.; Ward, T. L.; Rieker, T.; Brinker, C. J. Aerosol-Assisted Self-Assembly of Mesostructured Spherical Nanoparticles. *Nature* **1999**, *398*, 223−226.
(56) Godard, N.; Vivian, A.; Fusaro, L.; Cannavicci, L.; Aprile, C.; Debecker, D. P. High-Yield Synthesis of Ethyl Lactate with Mesoporous Tin Silicate Catalysts Prepared by an Aerosol-Assisted Sol-Gel Process. *ChemCatChem* **2017**, *9*, 2211−2218.
(57) Areva, S.; Boissière, C.; Grosso, D.; Asakawa, T.; Sanchez, C.; Lindén, M. One-pot aerosol synthesis of ordered hierarchical mesoporous core-shell silica nanoparticles. *Chem. Commun.* **2004**, 1630−1631.
(58) Chaumonnot, A.; Tihay, F.; Coupé, A.; Pega, S.; Boissière, C.; Grosso, D.; Sanchez, C. New Aluminosilicate Materials with Hierarchical Porosity Generated by Aerosol Process. *Oil Gas Sci. Technol.* **2009**, *64*, 681−696.
(59) Nandiyanto, A. B. D.; Iskandar, F.; Okuyama, K. Macroporous Anatase Titania Particle: Aerosol Self-Assembly Fabrication with Photocatalytic Performance. *Chem. Eng. J.* **2009**, *152*, 293−296.
(60) Bini, F.; Rosier, C.; Saint-Arroman, R. P.; Neumann, E.; Dablemont, C.; de Mallmann, A.; Lefebvre, F.; Niccolai, G. P.; Basset, J.-M.; Crocker, M.; et al. Surface Organometallic Chemistry of Titanium: Synthesis, Characterization, and Reactivity of $(\vdots Si-O)_nTi(CH_2C(CH_3)_3)_{4-n}$(n= 1, 2) Grafted on Aerosil Silica and MCM-41. *Organometallics* **2006**, *25*, 3743−3760.
(61) Marchese, L.; Maschmeyer, T.; Gianotti, E.; Coluccia, S.; Thomas, J. M. Probing the Titanium Sites in Ti−MCM41 by Diffuse Reflectance and Photoluminescence UV−Vis Spectroscopies. *J. Phys. Chem. B* **1997**, *101*, 8836−8838.
(62) Marchese, L.; Gianotti, E.; Dellarocca, V.; Maschmeyer, T.; Rey, F.; Coluccia, S.; Thomas, J. M. Structure-functionality relationships of grafted Ti-MCM41 silicas. Spectroscopic and catalytic studies. *Phys. Chem. Chem. Phys.* **1999**, *1*, 585−592.
(63) Madhusudan Reddy, K.; Manorama, S. V.; Ramachandra Reddy, A. Bandgap Studies on Anatase Titanium Dioxide Nanoparticles. *Mater. Chem. Phys.* **2003**, *78*, 239−245.
(64) Thanoo, B. C.; Jayakrishnan, A. Preparation of Hydrogel Beads from Crosslinked Poly(Methyl Methacrylate) Microspheres by Alkaline Hydrolysis. *J. Appl. Polym. Sci.* **1990**, *39*, 1153−1161.
(65) Groen, J. C.; Peffer, L. A. A.; Pérez-Ramírez, J. Pore Size Determination in Modified Micro- and Mesoporous Materials. Pitfalls and Limitations in Gas Adsorption Data Analysis. *Microporous Mesoporous Mater.* **2003**, *60*, 1−17.
(66) Fraile, J. M.; García, J. I.; Mayoral, J. A.; Vispe, E.; Brown, D. R.; Naderi, M. Is MCM-41 Really Advantageous over Amorphous Silica? The Case of Grafted Titanium Epoxidation Catalysts. *Chem. Commun.* **2001**, 1510−1511.
(67) Brutchey, R. L.; Ruddy, D. A.; Andersen, L. K.; Tilley, T. D. Influence of Surface Modification of Ti−SBA15 Catalysts on the Epoxidation Mechanism for Cyclohexene with Aqueous Hydrogen Peroxide. *Langmuir* **2005**, *21*, 9576−9583.
(68) Kochkar, H.; Figueras, F. Synthesis of Hydrophobic TiO_2-SiO_2 Mixed Oxides for the Epoxidation of Cyclohexene. *J. Catal.* **1997**, *171*, 420−430.
(69) Deo, G.; Turek, A. M.; Wachs, I. E.; Huybrechts, D. R. C.; Jacobs, P. A. Characterization of Titania Silicalites. *Zeolites* **1993**, *13*, 365−373.
(70) Jarupatrakorn, J.; Tilley, T. D. Silica-Supported, Single-Site Titanium Catalysts for Olefin Epoxidation. A Molecular Precursor Strategy for Control of Catalyst Structure. *J. Am. Chem. Soc.* **2002**, *124*, 8380−8388.
(71) Chiker, F.; Launay, F.; Nogier, J. P.; Bonardet, J. L. Green and selective epoxidation of alkenes catalysed by new TiO_2-SiO_2 SBA mesoporous solids. *Green Chem.* **2003**, *5*, 318−322.
(72) Mutter, R.; Dutoit, D. C. M.; Mallat, T.; Schneider, M.; Baiker, A. Novel mesoporous titania-silica aerogels highly active for the selective epoxidation of cyclic olefins. *J. Chem. Soc., Chem. Commun.* **1995**, 163−164.
(73) Lafond, V.; Mutin, P. H.; Vioux, A. Non-hydrolytic sol-gel routes based on alkyl halide elimination: toward better mixed oxide catalysts and new supports. *J. Mol. Catal. A: Chem.* **2002**, *182-183*, 81−88.
(74) Styskalik, A.; Skoda, D.; Pinkas, J.; Mathur, S. Non-Hydrolytic Synthesis of Titanosilicate Xerogels by Acetamide Elimination and Their Use as Epoxidation Catalysts. *J. Sol-Gel Sci. Technol.* **2012**, *63*, 463−472.
(75) Jorda, E.; Tuel, A.; Teissier, R.; Kervennal, J. Synthesis, Characterization, and Activity in the Epoxidation of Cyclohexene with Aqueous H_2O_2 of Catalysts Prepared by Reaction of TiF_4 with Silica. *J. Catal.* **1998**, *175*, 93−107.
(76) Gao, X.; Bare, S. R.; Fierro, J. L. G.; Banares, M. A.; Wachs, I. E. Preparation and In-Situ Spectroscopic Characterization of Molecularly Dispersed Titanium Oxide on Silica. *J. Phys. Chem. B* **1998**, *102*, 5653−5666.
(77) De Clercq, R.; Dusselier, M.; Poleunis, C.; Debecker, D. P.; Giebeler, L.; Oswald, S.; Makshina, E.; Sels, B. F. Titania-Silica Catalysts for Lactide Production from Renewable Alkyl Lactates: Structure-Activity Relations. *ACS Catal.* **2018**, *8*, 8130−8139.
(78) De Clercq, R.; Dusselier, M.; Makshina, E.; Sels, B. F. Catalytic Gas-Phase Production of Lactide from Renewable Alkyl Lactates. *Angew. Chem., Int. Ed.* **2018**, *57*, 3074−3078.
(79) Hartmann, M.; Machoke, A. G.; Schwieger, W. Catalytic Test Reactions for the Evaluation of Hierarchical Zeolites. *Chem. Soc. Rev.* **2016**, *45*, 3313−3330.